Boundary Layer Separation Control on the NACA 0012 Airfoil by using Triangular Rib Experimentally

التحكم بأنفصال الطبقة المتاخمة على الجنيح ذو رقم ناكا 0012 بأستخدام ضلع مثلث عمليا

Dr. Mohammed Wahhab Al-Jibory [1], Hussain Abed Ali Shinan[2]
[1, 2] Iraq, Kerbala University, Engineering College, Mechanical Engineering Department
[1]E-Mail: Dr.Mohammad.wahab@uokerbala.edu.iq
[2]E-Gmail: huss1982ain@gmail.com

Abstract:

This research paper introduces an experimental study to show a triangular rib effect on the aerodynamic characteristics of the NACA 0012 foil or wing. The study was done by using an open subsonic wind tunnel at a free stream velocity of 7 m/s (Reynold number=78,000) and a variable attack angle (0 to 22) degree. The triangular rib used in this study was located on the wing's upper surface at 90% of the total foil chord from the leading edge with a size of 4% of the total chord length. The results indicated that use of the triangular rib has a negative effect for the airfoil characteristics at the low angles of attack but, it becomes a positive when the attack angle increases above the 12-degree. Where, at the angle of 14˚, it enhances the lift, drag and performance of the wing approximately 18.5%, 20% and 47.8% respectively comparing with the smooth wing case. Through the comparison between results of this research and Ref. [12] results, it was noted there is a good agreement between them and a maximum deviation ratio was noted between them is about 23% at 16 degree an angle of attack.

Keywords: Passive technique, triangular rib, attack angle, lift, airfoil performance.

الخـــــــــلاصة:

هـذه الورقة البحثية تقدم دراسة عملية لبيان تأثير ضلع مثلث الشكل على خصائص الايروداينمك للجنيح او الجناح المرقم 0012 ناكا. الدراسة تمت بأستعمال نفق هوائي مفتوح عند سرعة تيار حر 7 م/ث (رقم رينولد 78,000) وزواية هجوم متغيرة من (0 الى 22) درجة. الضلع المستخدم في هذه الدراسة تم وضعه على السطح العلوي للجناح عند 90% من طول الوتر الكلي من الحافة الامامية بحجم 4% من طول الوتر الكلي. النتائج أشارت بأن أستخدام الضلع المثلث يمتلك تأثير سلبي بالنسبة لخصائص الجناح عند زوايا الهجوم المنخفضة و يصبح أيجابي عندما زاوية الهجوم تزداد فوق ال 12 درجة. حيث عند زاوية هجوم 14 درجة يحسّن الرفع، السحب واداء الجناح تقريباً 18.5% ، 20% و 47.8% توالياً بالمقارنة مع حالة الجناح الأعتيادي (الغير محدّث). من خلال المقارنة بين نتائج هذا البحث ونتائج المصدر [12]، لوحظ هناك توافق جيد بينهما وأعظم نسبة أنحراف لوحظت بينهما هي 23% عند زاوية هجوم 16 درجة.

Nomenclature

Symbol	Description	Units
c	Chord length of an airfoil	m
C_A	Axial force coefficient	
C_D	Drag force coefficient	
C_L	Lift force coefficient	
C_N	Normal force coefficient	
C_L/C_D	Lift to drag ratio (Airfoil's performance coefficient)	
C_P	Pressure coefficient	
C_{Pi}	Pressure coefficient at the point of i	
C_{Pj}	Pressure coefficient at the point of j	
H_i	Local pressure at the point of i of the airfoil surface	mm
H_s	Static pressure of the upstream flow	mm
H_t	Total pressure of the upstream flow	mm
P_d	Dynamic pressure of an upstream flow	Pascal
P_i	Local pressure at the point of i	Pascal
P_s	Static pressure of the upstream flow	Pascal
Re	Reynold number	
t	Airfoil's thickness	m
u_∞	Free stream velocity	m/s
w	Triangular rib's width	mm
x	Airfoil's chord length function	m
x_i	Location of the point (i) on the airfoil surface in the x coordinate	m
y	Airfoil's thickness function	m
y_i	Location of the point (i) on the airfoil surface in the y coordinate	m
Δx_{ij}	Horizontal distance between two points (i and j) in the x coordinate	m
Δy_{ij}	Normal distance between two points (i and j) in the y coordinate	m
α	Angle of Attack	Degree
ρ	Air Density	Kg/m^3
Abbreviations		
AOA	Angle of Attack	
APC	Airfoil's performance coefficient	
CNC	Computerized Numerical Control	
NACA	National Advisory Committee of Aeronautics	

1. Introduction

The air flow around the foil's surface at the low attack angles and velocities is a laminar and attached to the surface but at these angles, the airfoil's body (especially the symmetric airfoils) cannot generate a lift force in the form that allows the aircraft to be raised. On the other hand, when the attack angle is increased, the airflow becomes a turbulent leading to increase of the pressure difference between the upper and lower surface of the foil leading to the lift increase arrival to the critical value of this angle which is known by the stall angle at which the airfoil or wing produces a maximum lift force.

But, after that angle, the lift falls and the drag continue in the increase this because of the adverse pressure gradients generated due to the flow separation from the foil's surface. Hence, the flow separation control is considered an effective method to improve the aerodynamic characteristics of the foil.

The research aim is to improve the aerodynamic characteristics of the NACA0012 foil or wing (the lift, drag and performance of the airfoil) by removing or reducing separation area of the airflow and repeating this area to the work through, using a triangular rib on the upper surface of the wing.

To achieve this aim, there are some activities must be done as flow as: -

i. Determining coefficients of the lift, drag and performance of the wing (foil) by using the subsonic open wind tunnel with and without the triangular rib on the wing's upper surface.
ii. Comparing the results with and without the triangular rib to see how the airfoil or wing behaves with presence of that rib.
iii. Comparing results of the present work with previous studies to show accuracy and convergence of the present results.

2. Literature Review

In 2005, characteristics of the NACA 0012 airfoil were investigated experimentally by [1]. The investigation was done by using 200 V-grooves. The results indicated that the drag reduces about 6.5% by using that technique at an air velocity of 3m/s comparing with the smooth airfoil.

In 2012, [2] studied the aerodynamic performance of the NACA 65-021 and NACA 0021 airfoil experimentally without and with sinusoidal protrusions at the leading-edge of the airfoil at Reynolds number of 120,000 and different incidence angles. The results demonstrated that the airfoil's performance improves with the protrusions technique specially the NACA65-021 airfoil.

In an experimental study, a distributed roughness with different sizes at the leading-edge was used to improve the airfoil's performance at different Reynolds numbers (78,000, 169,000 and 230,000) and different attack angles from 0˚ to 18˚, in 2013, by [3]. It was found, for all the cases, that the maximum lift reduces and this reduction increases as Reynold number increases specially with the large size of roughness where reaches to 38%.

[4], in 2012, investigated experimentally the aerodynamic performance of NACA 4315 airfoil using a rough surface (partially bumpy). The study was done by adding that surface on the airfoil's upper surface with a height of 6.35 mm (2.5%c) at angles of attack from 0˚ to 20˚ and a chord of 26 cm. The results showed that using that technique improves the airfoil's performance by increasing the lift through delaying the flow separation about 6˚ but, it becomes ineffective at the high attack angles (greater than 19˚).

In an experimental study, vortex-generators were used to improve the aerodynamic performance of the NACA 23012 and 63_2217 airfoils, in 2015, by [5]. The results indicated

for the NACA 23012, there is an increase in the maximum lift about 14% and the drag do not increase for 2° of the attack angle and, in case of the NACA 63_2217, the increase in the maximum lift is 9% and the drag do not increase for 3° of the attack angle.

In 2016, an effect of the cylindrical pins for the NACA 0012 flapped airfoil's performance was studied experimentally by [6] through delaying the flow separation on the upper surface at different Reynolds numbers. The results showed that technique of the pins can reduce the separation region and increase the lift therefore, can improve the performance.

[7], in 2018, examined experimentally the NACA 0012 airfoil's performance without and with shark skin-inspired denticles at Reynolds number of 40,000, a variable attack angle from 0˚ to 24˚ and the airfoil chord length of 68 mm. The results proved that using that technique leads to reduction in the drag and increase in the lift therefore, there is large improvement in the aerodynamic performance of airfoil.

The aerodynamic efficiency of NACA 0012 airfoil without and with dimples was studied experimentally, in 2017, by [8]. The study was carried out by applying the dimples at 30%c from the trailing edge, at conditions; 6 and 10 m/s an air velocity, 30 cm the chord length, from 0 to 23-degree range of attack angles and 1%c, 2%c and 3%c size of dimpled surface. It was found that the efficiency of airfoil improves with the dimples.

[9], in 2018, investigated experimentally effect of the trips for the NACA 0012 airfoil's performance. The investigation was done by using the tripwires at the airfoil leading edge with different diameters (2, 1.6, 1.2, 0.95) mm at 20,000 Reynolds number and different attack angles. The results showed that technique of the tripwires improves efficiency of the airfoil for a wide range of attack angles but, it becomes ineffective after the stall angle because of the flow separation completely.

[10], in 2019, used dimples as a passive technique, in an experimental and numerical study, to control the flow separation on the $NACA64_2 - 014A$ airfoil's surface at Reynolds number of 175,000. It was noted that using that technique reduces the separation region and the drag.

3. Experimental Apparatuses and Setup

3.1 Subsonic Wind Tunnel

It is the main test apparatus in which all the experiments are conducted to investigate the air flow around the wing and contains auxiliary devices as shown in the diagram in the figure (1).

In this work, all the experiments were done in the subsonic open-circuit wind tunnel C2-00 presented in **University of Babylon, Department of Mechanical Engineering** which has overall length of 2.98 m, overall height of 1.83 m, overall width of 0.8 m and test section of 300 mm × 450 mm.

3.2 Measurement Devices

3.2.1 Multi-Tubes Manometer

It is the device which is used to measure the static pressure distribution on both two surfaces of the wing through the water height (mm) in each tube where each tube in the manometer device (20 tubes) is connected to one hole on the wing's surface by special connections (2 mm diameter). The water in this device has a density of 1000 kg/m^3.

3.2.2 Pitot-Static Tube

The purpose of using this device is to measure the total and static pressure at the test section inlet (before the wing). It has diameter of 4 mm and length of 40 cm. Figure (2) shows the schematic diagram and plate of the pitot-static tube.

3.3 Test Model

The test model used in this study is the NACA0012 wing. It was designed by the SolidWorks software with dimensions of 168 mm the chord length and 300 mm the span length. Knowing that coordinates of the NACA 0012 airfoil (x and y) were governed by the equation (1) [11].

By CNC machine and from the wood material, the wing was manufactured with two symmetric parts where, in each part, pressure taps with small diameters (1.5mm) were installed with different distances for measuring the pressure distribution around the wing surface and after joining the two parts together and performing the model and smoothing it, the wing was installed within the test section of the open wind tunnel. Figure (3) shows steps of the wing manufacture and its installing inside the test section.

$$\mp y = 5tc\left\{T_1\left(\sqrt{x/c}\right) - T_2\,(x/c) - T_3(x/c)^2 + T_4(x/c)^3 - T_5(x/c)^4\right\} \quad \ldots (1)$$

Where: $T_1 = 0.2969$, $T_2 = 0.126$, $T_3 = 0.3516$, $T_4 = 0.2843$ and $T_5 = 0.1015$.

3.4 Triangular Rib

The triangular rib used in this research to enhance the aerodynamic characteristics of the wing which has a cross-section shown in the figure (4 a) was manufactured from the iron material with equaled dimensions for the cross-section (h=w=4% of the total chord length) and a length of 30 cm. After that, it was installed on the upper surface of the wing at the location of 90% of the chord length from the leading edge as shown in the figure (4 b).

3.5 Experimental Procedure

- Measuring the atmospheric pressure and the temperature inside the laboratory before conducting the experimental tests.
- Installing the wing inside the test section of the wind tunnel and setting it with the required attack angle.
- Connecting the pressure pipes exiting from the test section to the multi-tube manometer device by appropriate connections and check them well before operating the wind tunnel.
- Preparing the multi-tubes manometer device and determine the water level.
- Operating the wind tunnel with the waiting for five minutes in order to the water level becomes stable.
- Setting the fan by the velocity control at the required velocity for conducting the investigation.
- Recording the new water level in the manometer device for finding the pressure distribution on both two surfaces of the model.
- Repeating the process with each new attack angle.
- Taking the readings for different angles of attack from the zero to 22˚.
- Repeating the process for the modified airfoil with the triangular rib.

4. Boundary Conditions

All the experimental calculations were done at the following boundary conditions: -

a. The air velocity at input of the test section ($u_\infty = 7\ m/s$),
b. Density of the air (ρ =1.21 kg/m^3),
c. Air dynamic viscosity (μ =1.8243 e-5 kg/m s),
d. Constant air temperature (T=298 k),
e. The heat capacity ratio of the air (K=1.4).

Then Reynold number according to these conditions and the equation (11) equals 78,000.

$$Re_c = \frac{\rho u_\infty c}{\mu} \qquad \dots (2)$$

5. Experimental Calculations

After executing the tests and taking the readings at a velocity of 7 m/s (Re=78,000) and different attack angles (0, 10, 12, 14, 16, 18, 20 and 22) with and without the triangular rib, the experimental calculations were done as following:

1) Through, the water heights in the Multi-Tubes Manometer, the static and total pressure measured by Pitot-static tube, the pressure coefficients were calculated by the following equation:

$$C_P = \frac{2(P_i - P_s)}{\rho U_\infty^2} = \frac{Hi - H_s}{H_t - H_s} \qquad \dots (3)$$

2) The average pressure coefficients between a hole and other on the wing's surface were determined by the following equation (continue motion about the wing's surface from the leading edge of upper surface to the leading edge of the lowest surface) where (j=i+1).

$$C_{Pij} = \frac{C_{Pi} + C_{Pj}}{2} \qquad \dots (4)$$

3) The distances between a hole and other were determined for both the two directions (x and y) as following:

$$\Delta x_{ij} = x_j - x_i \qquad \dots (5)$$

$$\Delta y_{ij} = y_j - y_i \qquad \dots (6)$$

4) After that, coefficients of the normal and axial forces were calculated as following:

$$C_N = -\frac{1}{c} \sum_{\left[\substack{For\ all\ Panels \\ (goning\ CCW)}\right]} C_{P\,ij} \times \Delta x_{ij} \qquad \dots (7)$$

$$C_C = \frac{1}{c} \sum_{\left[\substack{For\ all\ Panels \\ (goning\ CCW)}\right]} C_{P\,ij} \times \Delta y_{ij} \qquad \dots (8)$$

5) Then, and through, results of the normal and axial coefficients, the lift and drag coefficients were calculated as following:

$$C_L = C_N \cos\alpha - C_A \sin\alpha \qquad \dots (9)$$

$$C_D = C_N \sin\alpha + C_A \cos\alpha \qquad \dots (10)$$

From results of the lift and drag coefficients, the NACA 0012 airfoil's aerodynamic performance coefficient (APC) can be determined by finding the lift to drag ratio as following:

$$APC = C_L / C_D \qquad \dots (11)$$

6. Results, Discussion and Comparison

6.1 Pressure Distribution

Figures (5), (6) and (7) show results of the pressure distribution in terms of the pressure coefficients around the smooth and modified wing with the triangular rib with a size of 4%c and location of 90%c at the angles of attack 10˚, 14˚ and 18˚ respectively.

The results showed as follow as: -

At 10˚ an angle of attack and in the smooth wing case, there is a full attachment of the airflow on the upper surface of the wing this is a clear through the pressure distribution on two surfaces of the wing and the rib presence on the upper surface causes increase in the pressure on that surface see figure (5).

At 14˚ and in case of the smooth wing, the flow separation is a clear through decrease of the pressure difference between the two surfaces while, this difference increases with the rib presence see figure (6) since using the rib breaks the vortices generated due to the separation.

At 18˚ the rib effect, for the pressure distribution, is a small since the vortex size becomes a very large and the rib presence with the present conditions cannot break that vortex.

6.2 Lift, Drag and Performance Coefficients of the Wing

The lift, drag and performance coefficients of the NACA0012 wing without and with the triangular rib on the wing's upper surface with the size of 4% at the location of 90%c, were calculated and compared as shown in the figures (8) and (9) respectively after calculation of the pressure, normal and axial coefficients.

The results showed as follow as: -

At the low angles of attack ($\alpha < 12^{\circ}$), the triangular rib effect is a negative for results of the lift, drag and performance because the wing, at these angles, works with its surface area completely and correctly.

At the angle of 12˚, the rib has a positive effect only for the lift results and a very small effect (negative) for the drag results therefore, there is a small enhancement in the performance since, at that angle, the flow separation is presented but, with a small size of bubble.

While, at the higher angles ($\alpha > 12^{\circ}$), there is a large increase in the lift and reduction in the drag therefore, there is a large enhancement in the wing's performance because the rib was used with correct and suitable size and location for the separation bubble at these angles, specially at the angle of 14˚, where the rib presence on the wing's surface, at that angle, improvs the lift, drag and performance of the wing approximately 18.3%, 20% 47.8% respectively comparing with the smooth wing.

But, at ($\alpha > 20^{\circ}$), the rib effect for the wing's characteristics under these conditions becomes a very small because the separation bubble size becomes a very large.

6.3 Results Comparison

Figure (10) involves a comparison of results of the lift and drag coefficients of the present work with Ref. [12] for a wide range of the angles of attack (0 to 18) degree at Reynolds numbers of 78,000 and 100,000 respectively.

Where, it was noted there is a large agreement between them although, the present work is an experimental study and the research of [12] is a numerical study and difference of some the test conditions. And a maximum deviation ratio was noted between them is about 23% at 16 degree an angle of attack.

7. Conclusions

In this study, the air flow around the NACA0012 wing surface was investigated experimentally by using the subsonic open-circuit wind tunnel at Reynold number of 78,000 (7 m/s air velocity) and different angles of attack (from 0 to 22) degree without and with the triangular rib technique.

It was concluded that using that technique greatly relates with the angle of attack. So, at the low angles, leads to negative results for the lift, drag and wing's performance but, at the high angles, becomes a very useful. Where, at the angle of 14˚, leads to an enhancement in the lift, drag and performance of the wing approximately 18.3%, 20% and 47.8% respectively.

References

[1] S. Ã. Lee and Y. Jang, "Control of flow around a NACA 0012 airfoil with a micro-riblet film" Journal of Fluids and Structures, vol. 20, pp. 659–672, 2005.

[2] K. L. Hansen, R. M. Kelso, and B. B. Dally, "Performance Variations of Leading-Edge Tubercles for Distinct Airfoil Profiles," *AIAA J.*, vol. 49, no. 1, pp. 185–194, 2012.

[3] Y. Zhang, T. Igarashi, and H. Hu, "Experimental Investigations on the Performance Degradation of a Low-Reynolds-Number Airfoil with Distributed Leading Edge Roughness," no. January, pp. 1–18, 2014.

[4] M. Mashud and H. Ali, "Role of Partially Bumpy Surface To Control The Flow Separation Of An Airfoil," vol. 7, no. 5, pp. 584–587, 2012.

[5] V. del Campo, D. Ragni, D. Micallef, J. Diez, and C. J. Simão Ferreira, "Estimation of loads on a horizontal axis wind turbine," *Wind Energy*, vol. 18, no. 11, pp. 1875–1891, 2015.

[6] S. Gildersleeve, D. Clingman, and M. Amitay, "Separation Control over a Flapped NACA 0012 Model using an Array of Low Aspect Ratio Cylindrical Pins," no. June, pp. 1–19, 2016.

[7] G. Domel, K. Bertoldi, M. Saadat, G. V. Lauder, J. C. Weaver, and H. Haj-Hariri, "Shark skin-inspired designs that improve aerodynamic performance," *J. R. Soc. Interface*, vol. 15, no. 139, pp. 1–9, 2018.

[8] S. K. Rasal and R. R. Katwate, "Experimental Investigation Of Lift & Drag Performance of NCAC 0012 Wind Turbine Aerofoil," pp. 265–270, 2017.

[9] R. R. Leknys, M. Arjomandi, R. M. Kelso, and C. H. Birzer, "Journal of Wind Engineering & Industrial Aerodynamics Thin airfoil load control during post-stall and large pitch angles using leading-edge trips," Journal of Wind Engineering & Industrial Aerodynamics, vol. 179, no. May, pp. 80–91, 2018.

[10] V. D'Alessandro, G. Clementi, L. Giammichele, and R. Ricci, "Assessment of the dimples as passive boundary layer control technique for laminar airfoils operating at wind turbine blades root region typical Reynolds numbers," *Energy*, vol. 170, pp. 102–111, 2019.

[11] O. Obiga and B. E. Hons, "Investigation of the Performance of a Slotted Aerofoil at Low Reynolds Numbers," no. October, 2016.

[12] L. Huang, P. G. Huang, R. P. LeBeau, and T. Hauser, "Numerical Study of Blowing and Suction Control Mechanism on NACA0012 Airfoil," J. Aircraft., vol. 41, no. 5, 2003.

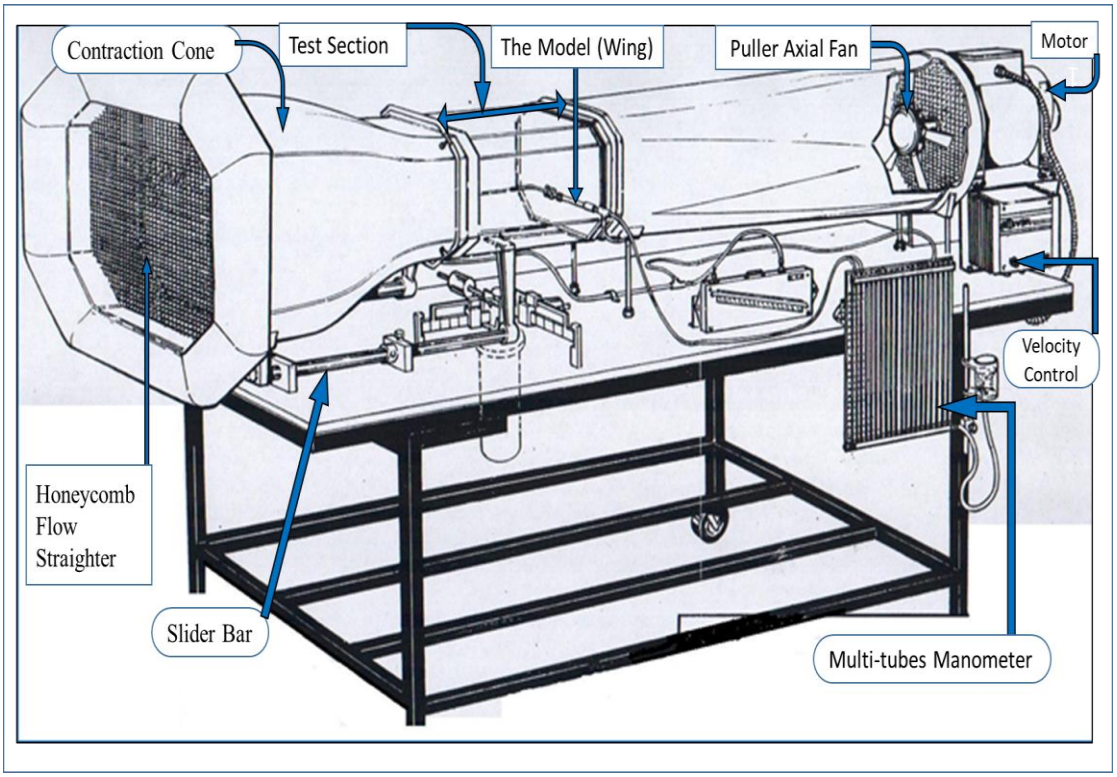

Figure (1): Schematic Diagram of the Wind Tunnel and the Auxiliary Devices.

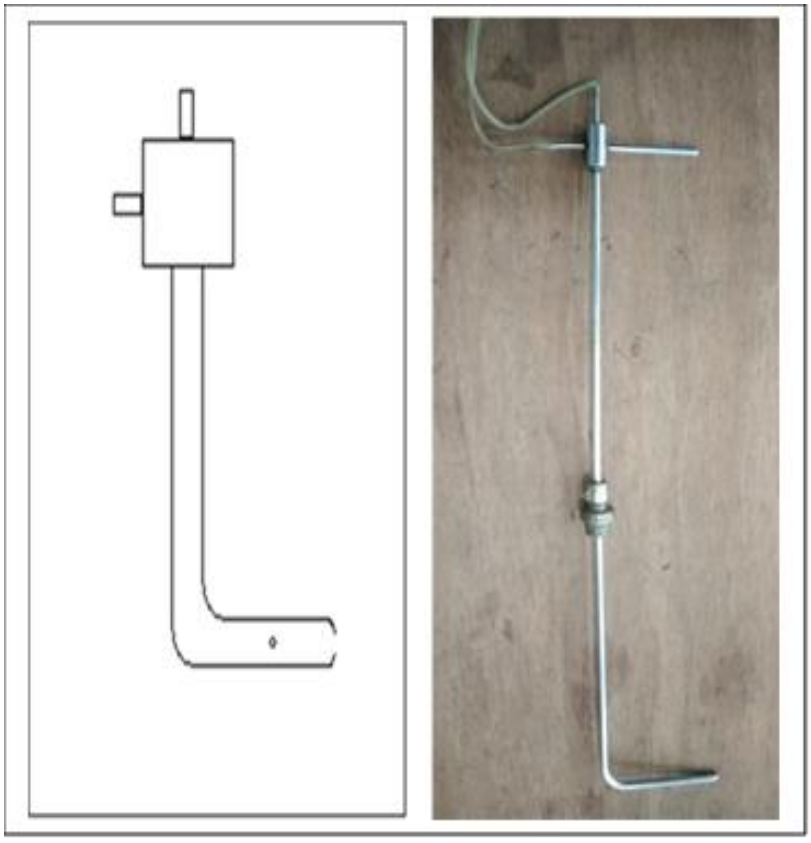

Figure (2): Schematic Diagram and Plate of the Pitot-Static Tube.

Figure (3): Steps of the Wing Manufacture and Installation it inside the Wind Tunnel.

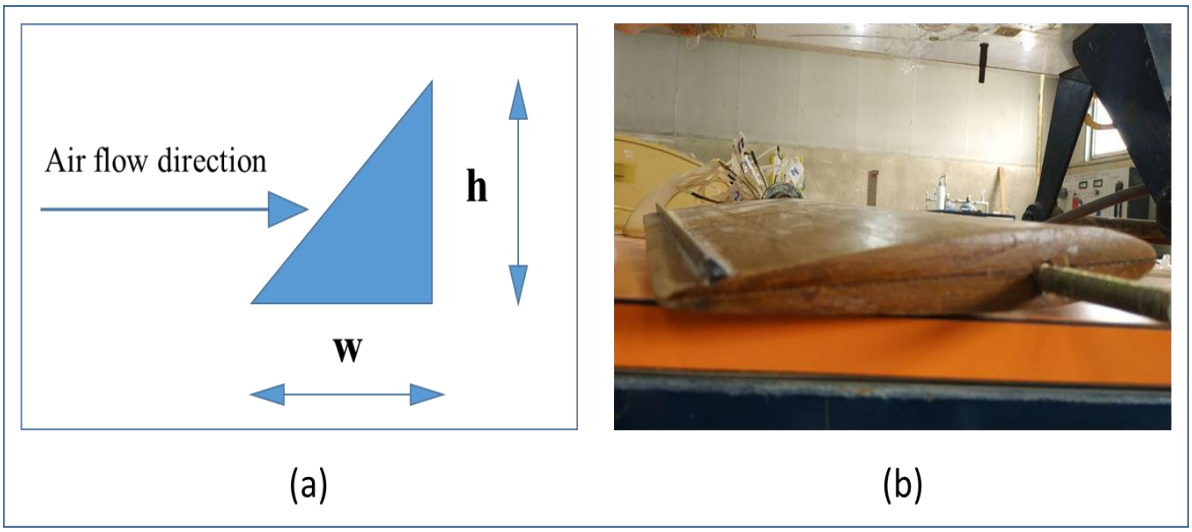

Figure (4): (a) Cross-section of the Triangular Rib and (b) Modified Wing with the Rib.

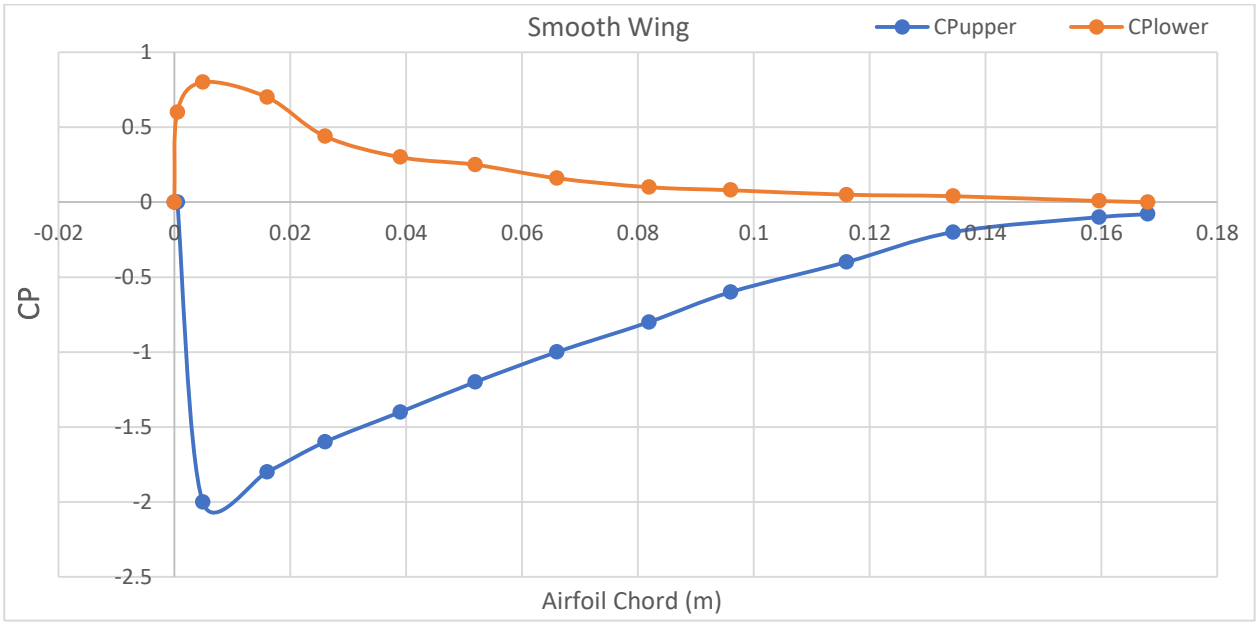

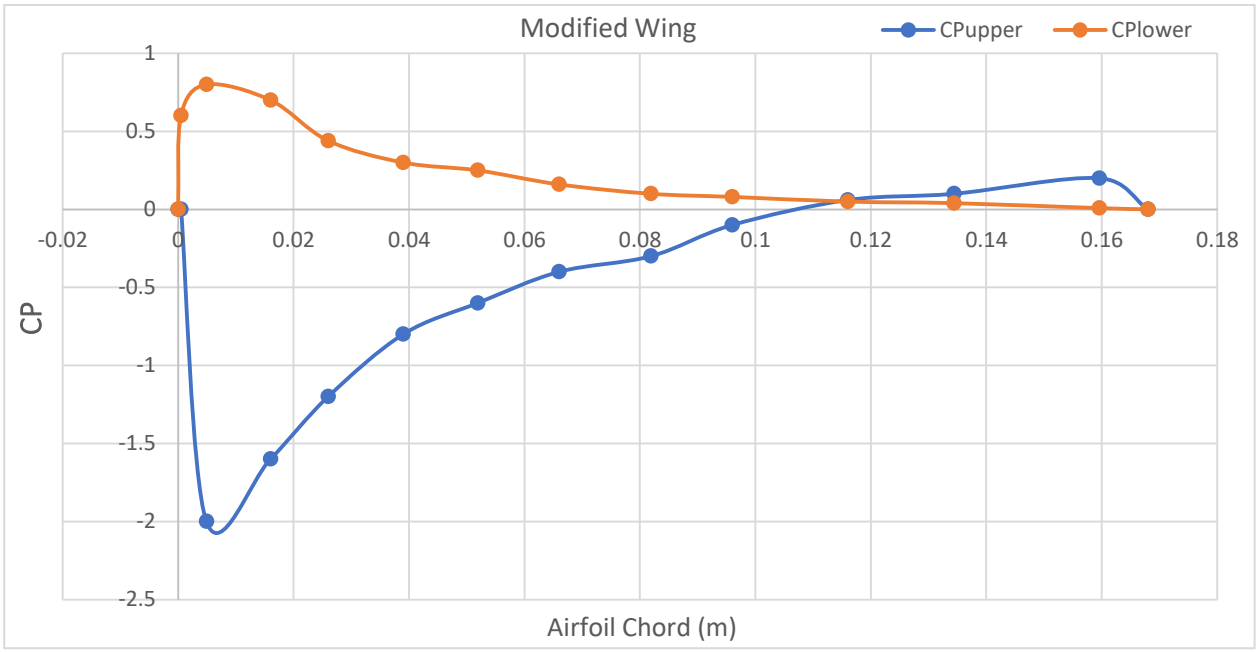

Figure (5): The Pressure Distribution (CP) around Surface of the Smooth and Modified Wing at Attack Angle of 10˚.

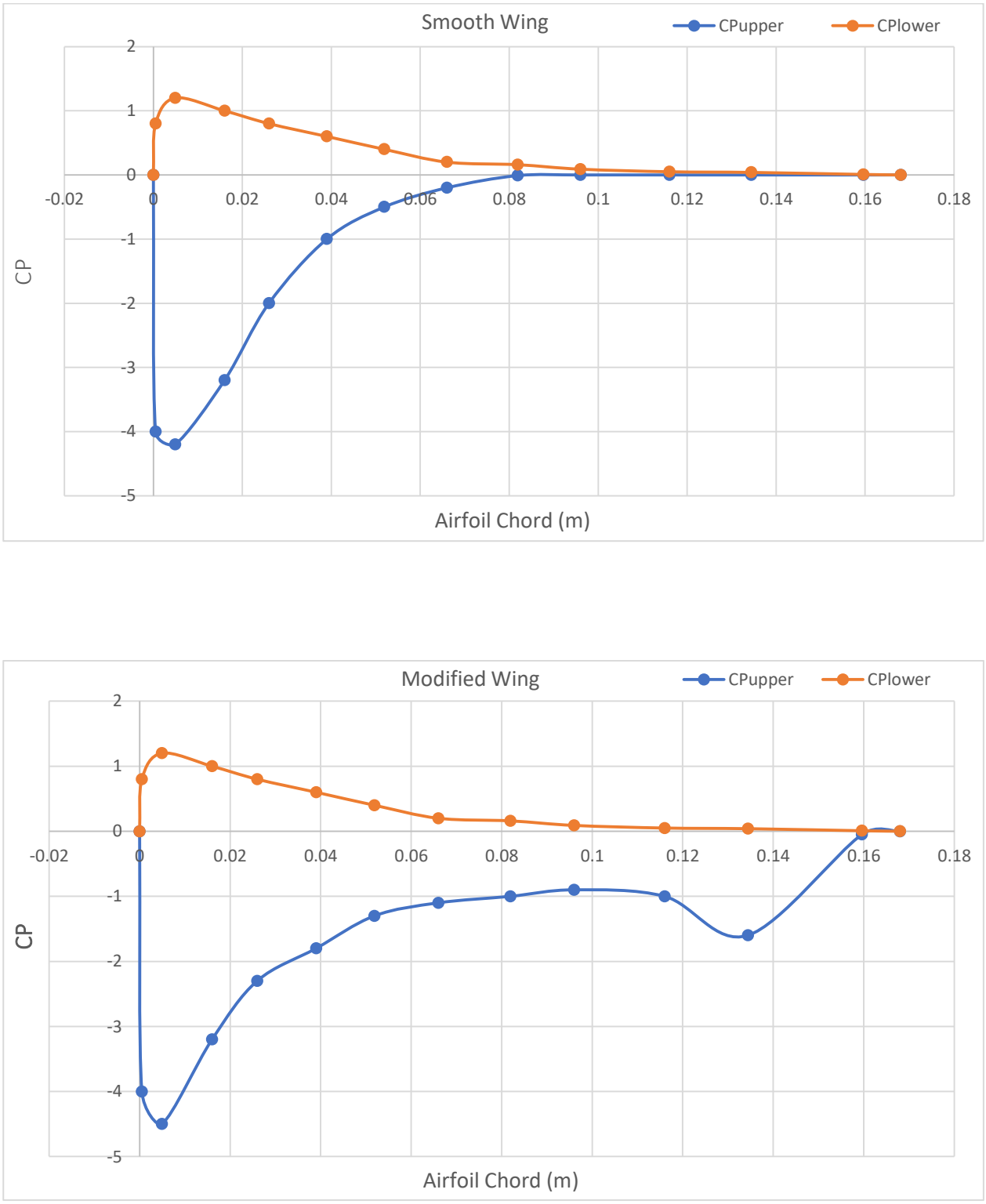

Figure (6): The Pressure Distribution (CP) around Surface of the Smooth and Modified Wing at Attack Angle of 14˚.

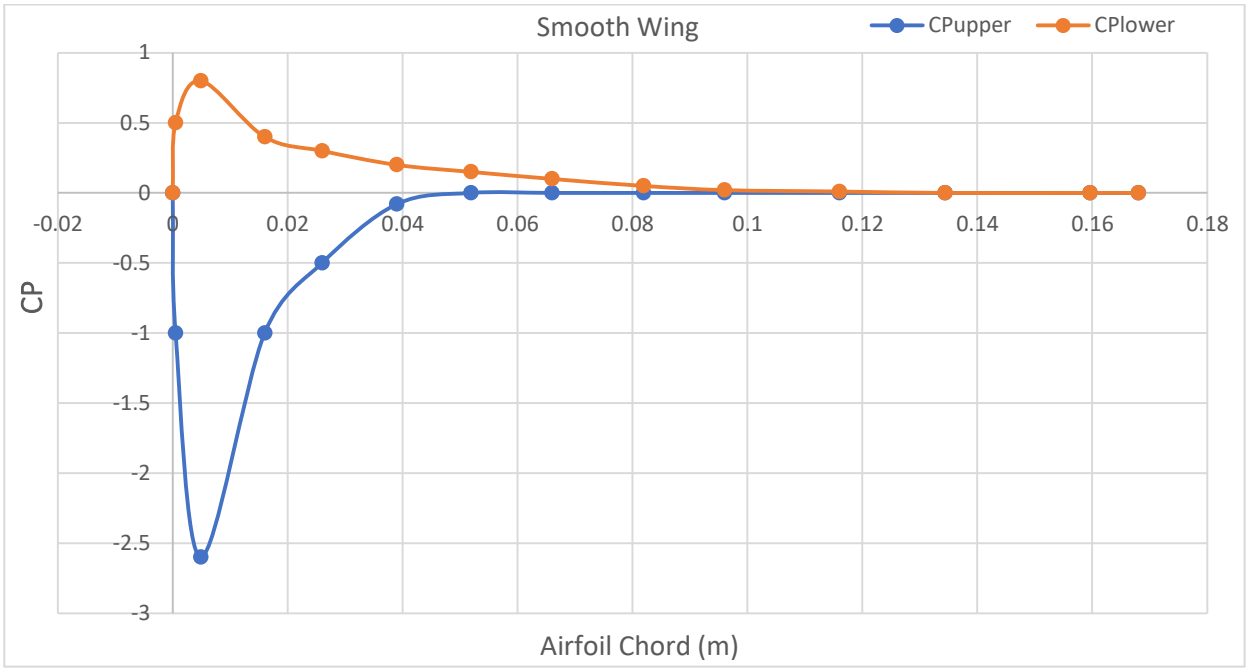

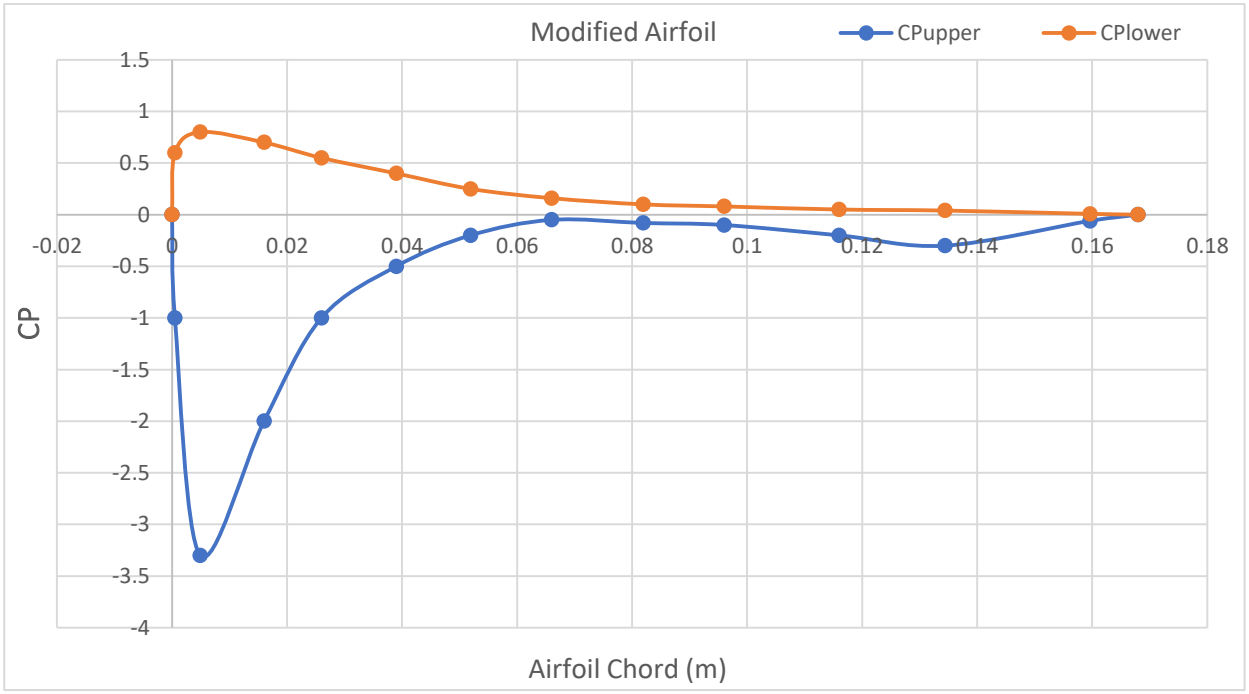

Figure (7): The Pressure Distribution (CP) around Surface of the Smooth and Modified Wing at Attack Angle of 18˚.

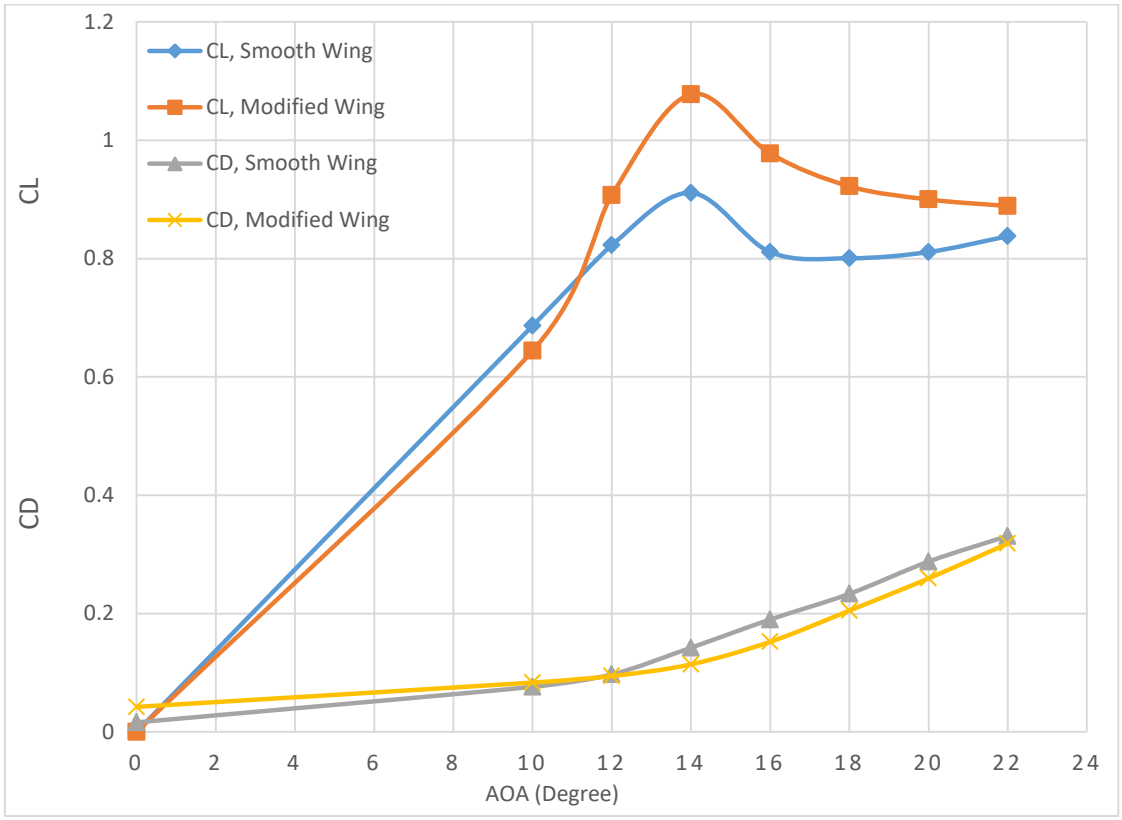

Figure (8): The Lift and Drag Coefficients without and with the Triangular Rib with the 4%c Size and 90%c Location versus the Attack Angle.

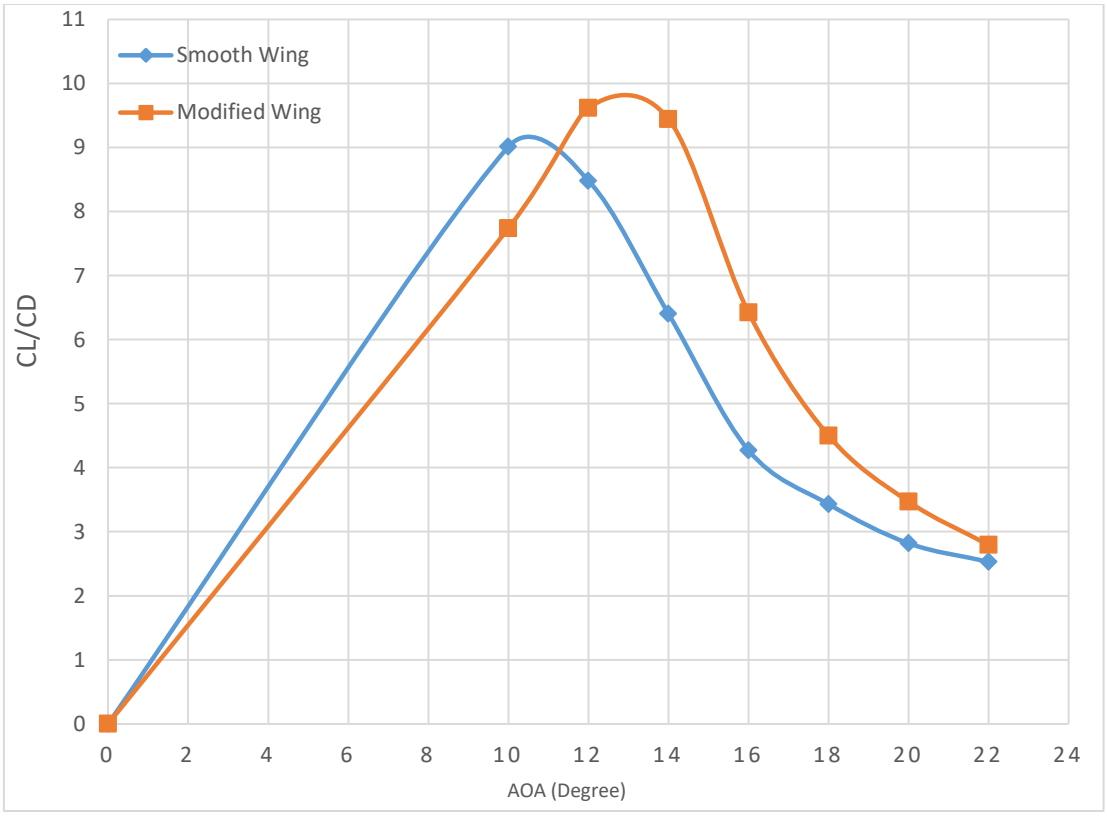

Figure (9): The Performance Coefficient of the Wing (CL/CD) without and with the Triangular Rib with the 4%c Size and 90%c Location versus the Attack Angle.

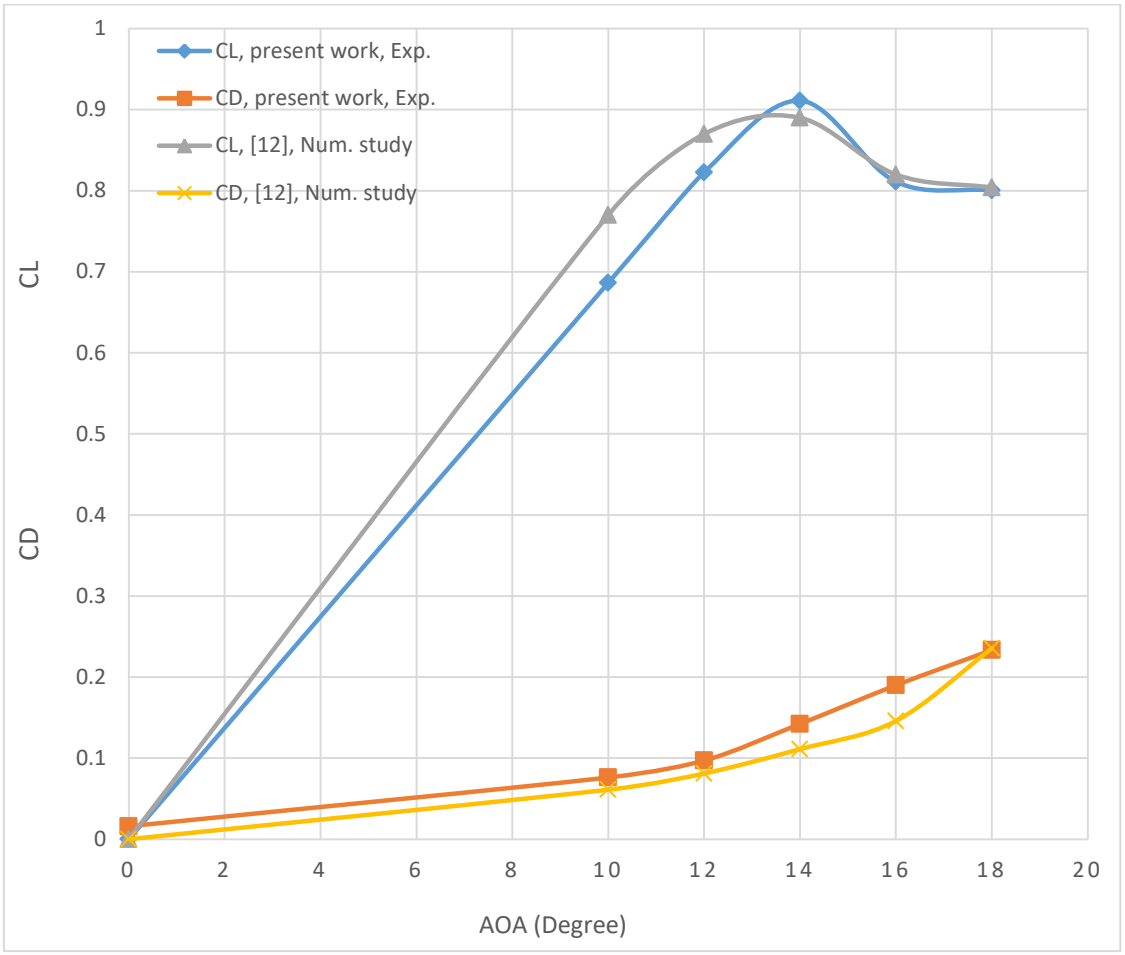

Figure (10): Results Comparison of the Lift and Drag Coefficients of the Present Work with Ref. [12].